Available online at www.sciencedirect.com
SCIENCE DIRECT®
Journal of Applied Geophysics 52 (2003) 139–156
JOURNAL OF APPLIED GEOPHYSICS
www.elsevier.com/locate/jappgeo

# A combined seismic reflection and refraction study of a landfill and its host sediments

R. De Iaco, A.G. Green*, H.-R. Maurer, H. Horstmeyer

*Institute of Geophysics, ETH-Hoenggerberg, HPP-Gebaude, Zurich CH-8093, Switzerland*

Received 7 June 2001; accepted 9 December 2002

**Abstract**

In an attempt to delineate the base of a landfill and map the geometries of the host sediments, we have recorded a high-resolution seismic profile. To obtain sufficient resolution in the heterogeneous landfill environment, common midpoint (CMP) spacing was set to 0.125 m and subsurface coverage (i.e. fold) was maintained at $\geq 120$ in the central region of the survey. Despite the high density and high redundancy of the data, severe source-generated noise (i.e. direct, refracted, guided and surface waves) and strong lateral velocity variations made it difficult to identify reflections on processed shot and CMP gathers. However, a quasi-continuous sequence of reflections R1–R3 was eventually traced along the length of the profile. After time-to-depth converting the stacked seismic reflection section using poorly resolved initial stacking velocities, no consistent correlations with boundaries identified in nearby boreholes and on three-dimensional georadar data were apparent. In a first attempt to obtain more reliable velocities, ~183,000 first-arrival times were tomographically inverted. Unfortunately, the resultant velocity model was found to be incompatible with knowledge supplied by the borehole and georadar data and the seismic reflection section. By including the known depths to a key geological horizon and the R1–R3 traveltimes as constraints, a second suite of tomographic inversions produced a satisfactory model. This model included a thin capping layer of humus and sandy clay (velocities of 400–1000 m/s) overlying a distinctly lower velocity landfill (200–600 m/s) along the northern half of the profile and a southward thickening sequence of fluvial deposits (600–900 m/s) along the southern half. A southward thinning layer of compact lacustrine sediments and basal till (2000–3800 m/s) and a nearly horizontal bedrock interface (4000–5400 m/s) was mapped beneath the entire profile. Although independent applications of the seismic reflection and refraction techniques were not successful in meeting the survey objectives, a combination of the two approaches suitably constrained by borehole information finally provided the required details on the landfill and surrounding sediments. Nevertheless, our study has highlighted the limitations of employing 2-D seismic refraction and reflection methods for resolving problems in highly heterogeneous 3-D media.


*Keywords:* Landfill; Seismic reflection; Velocity

## 1. Introduction

Seismic refraction and reflection surveys have been conducted at a number of proposed landfill sites and

* Corresponding author. Tel.: +41-1-633-2657; fax: +41-1-633-1065.
*E-mail address:* alan@aug.ig.erdw.ethz.ch (A.G. Green).

0926-9851/03/$ - see front matter © 2003 Elsevier Science B.V. All rights reserved.
doi:10.1016/S0926-9851(02)00255-0

in the vicinity of several existing ones. Their purpose was to detect faults and fracture zones that may provide pathways for groundwater and contaminant transport and to map the geometry and lateral continuity of sediments and bedrock (Rodriguez, 1987; Slaine et al., 1990; Boyce et al., 1995; Doll et al., 1996; Lanz et al., 1998; Doll, 1998; Dana et al., 1999; Murray et al., 1999).

Since landfills are usually characterised by much lower velocities than the surrounding sediments, seismic refraction methods are also well suited for outlining their borders. Relatively simple processing and interpretation techniques may provide knowledge of a landfill's boundaries in a fast and inexpensive manner, (Cardarelli and Bernabini, 1997; Granda and Cambero, 1998), whereas sophisticated refraction tomography is capable of supplying detailed images (Lanz et al., 1998).

Reports of successful seismic reflection surveys across landfills are rare (Pasasa et al., 1998). There are a number of reasons why seismic reflection techniques may fail in landfill investigations:

1. high levels of scattering and anelastic attenuation cause unconsolidated wastes to be generally poor transmitters of seismic waves—high-frequency components, which are important for good resolution, are particularly affected by such processes;
2. source-generated noise (i.e. direct, refracted, guided and surface waves) may mask shallow reflections (Robertsson et al., 1996a,b; Roth et al., 1998);
3. strong lateral velocity variations may inhibit the recording of hyperbolic-shaped events, making identification of reflections difficult.

In this contribution, we present the results of a high-resolution seismic survey conducted across the 20-year-old Härkingen landfill and host sediments in north-central Switzerland (Fig. 1). We begin by outlining the geological environment and seismic data acquisition strategy. Problems encountered during the conventional seismic reflection processing of these data and uncertainties associated with the resultant seismic section are then described. To overcome these limitations, velocity models derived from tomographic inversions of first-arrival traveltime data are considered. Our preferred velocity model explains the traveltimes of first arrivals and the traveltimes of near-vertical-incident reflections interpreted to originate from a key geological boundary intersected in nearby boreholes.

## 2. Local geology and Härkingen landfill

Several boreholes within the study site illustrate the different stages of erosion and sedimentation that occurred during and after Riss glaciation 200,000–100,000 years ago (Figs. 1 and 2; Kissling, 1998). A 0.2–0.3-m thick surface layer of humus covers 10–16 m of heterogeneous fluvial sediments that include channels of sandy and silty gravel and isolated lenses of clean sand. These fluvial sediments, which contain an important 21-km$^2$ groundwater reservoir, are underlain by 3–5 m of compact sand, sandy silt and sandy clay deposited in a lacustrine environment. Beneath the lacustrine units are 0.5–6.3 m of till, representing an ancient basal moraine. Bedrock lies at a depth of $\sim$20 m. North of the landfill (borehole B1), bedrock comprises Lower Freshwater Molasse siltstone, whereas to the south it consists of an Upper Jurassic limestone sequence. A perched groundwater table deepens by $\sim$6 m over a distance of $\sim$125 m between borehole B9 and boreholes B2 and B8.

The extent of the Härkingen landfill, a former gravel pit that now contains mainly household/construction refuse with significant amounts of harmful industrial waste, is outlined by the dashed line in Fig. 1. Lateral boundaries of the landfill have been determined via magnetic, frequency-domain electromagnetic (EM31) and georadar investigations (De Iaco et al., 2000). None of these studies provided direct estimates of landfill thickness. Nevertheless, the georadar data revealed distinct layering within the fluvial gravel deposits and mapped the upper surface of lacustrine sediments beside the landfill. Since excavation in the former gravel pit would have ceased once the silt and clay were encountered, it is highly likely that the landfill base is no deeper than the natural upper surface of lacustrine sediments.

Old photographs and borehole information have demonstrated that gravel was excavated to below the perched groundwater table before the pit was transformed to a landfill. After its closure, the landfill was

covered by ~2 m of humus and sandy clay. Elevation across the seismic profile varied from 429.6 to 431.1 m (i.e. maximum difference of only 1.5 m).

## 3. Seismic data acquisition

Seismic data were recorded across the landfill and adjacent natural ground to the south (Fig. 1). Initially, walkaway tests were conducted with hammer, pipegun, weight drop and explosive sources. The hammer provided only weak signals over the soft ground and the frequency content of data generated by the weight drop was unsatisfactorily low. Detonation of closely spaced explosive charges would have been time-consuming and may have damaged the humus and sandy clay layers covering the landfill. Therefore, the relatively fast and inexpensive pipegun was chosen for the energy source. On the basis of the source tests, it was clear that the base of the landfill was going to be a difficult target to image. Consequently, we decided to acquire a high-resolution data set with high fold (Table 1).

Source locations were spaced at 0.25-m intervals. Twelve-gauge blank cartridges were detonated in water-filled holes at depths of 0.7–1.3 m within the landfill boundaries and 0.5–0.8 m in natural ground. A total of 859 shots was required to complete the survey (see Fig. 1 for shot locations). Geophones with natural frequencies of 30 Hz were spaced at 0.25-m intervals within the landfill boundaries and 0.5-m intervals over natural ground, They were connected to a 240-channel recording system. The target depth of 0–40 m was covered by source-receiver offsets ranging from 0 to 60 m. Effective roll-along was achieved by shooting through the first 24 geophones of a receiver spread (i.e. one cable) and then moving the first cable to the end of the spread. Since the dominant frequencies expected of reflections from the base of the landfill were unknown, no filters were applied during data acquisition. At each source point, 250 ms of data with a sampling interval of 0.25 ms were recorded. Subsurface coverage (i.e. fold) was $\geq 120$ over the distance range 30–168 m (Fig. 2). The entire survey, which

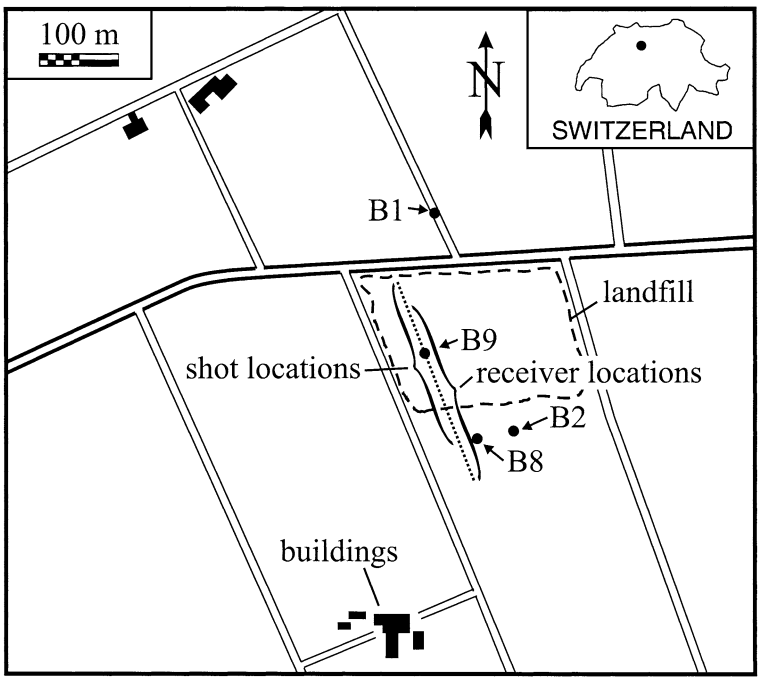


Fig. 1. Map of study area. Dashed lines outline landfill boundaries. Dotted line identifies seismic reflection profile; note locations of shots and receivers. Black dots mark positions of boreholes B1, B2, B8 and B9 (Kissling, 1998).

Table 1
Acquisition parameters

| | Landfill | Natural ground |
|---|---|---|
| Source | Pipegun (12-gauge blank cartridges) | Pipegun (12-gauge blank cartridges) |
| Source depths (m) | ~ 0.7–1.3 | ~ 0.5–0.8 |
| Receivers | 30Hz single geophones | 30Hz single geophones |
| Number of channels | 240 | 120 |
| Sampling interval (ms) | 0.25 | 0.25 |
| Record length (ms) | 250 | 250 |
| Nominal source spacing (m) | 0.25 | 0.25 |
| Receiver spacing (m) | 0.25 | 0.5 |
| Nominal CMP spacing (m) | 0.125 | 0.125 |
| Offset range (m) | 0.0–59.75 | 0.0–59.5 |
| Max. minimum offset (m) | 5.75 | 11.5 |
| Min. maximum offset (m) | 54.0 | 48.0 |

Fold was 120–190 at distances 30–168 m, and 0–120 at distances 0–30 and 168–240 m.

was conducted under cold, wet and muddy conditions, was accomplished in 8 days with a four- to five-person crew.

## 4. Identifying reflections in highly complex data

To interpret shallow events on stacked seismic sections, it is generally recognised that their origins need to be established through studies of raw and progressively processed prestack data (Steeples et al., 1997; Büker et al., 1998). Such an approach is particularly important for complex data sets in which reflections are difficult to distinguish from various forms of source-generated noise. A consequence of our analyses is that relatively ''brutal'' top-mute functions need to be applied before stacking the data.

Fig. 3a–c show trace-normalised raw data generated by shots at three different locations. Shot gathers 75 and 141 are located entirely over the landfill, whereas shot gather 696 crosses natural ground. These displays highlight the variable quality of the first-breaks F and demonstrates the dominance of low-frequency source-generated noise (i.e. guided and surface waves). Distinct hyperbolic-shaped events (e.g. R1 in Fig. 3a) are only observed on a limited number of raw shot gathers. Other possible specular reflections are overwhelmed by strong surface waves S in the near-offset range and by guided waves U in the far-offset range. Without further processing, and taken in isolation, none of the marked ''R'' events on Fig. 3a–c would be convincingly interpreted as reflections.

Scaling the raw data with a 30-ms AGC and applying a conservative F–K filter reduces the relative amplitudes of the surface and guided waves, thus, improving the visibility of events R1 and R2 and the high-frequency air wave A (Fig. 3d–f). Also more apparent is a first-break traveltime delay T, which is diagnostic of a velocity inversion in the shallow subsurface. The low-frequency surface waves are also attenuated relative to the higher frequency reflections and air waves by spectral balancing (30–45 to 250–400 Hz; Fig. 3g–i). The possible reflection R3 is apparent in Fig. 3i, but the surface waves remain prominent in this shot gather, indicating that higher frequency surface waves are generated in natural ground than within the landfill.

The generally higher frequency content of the possible reflections relative to the surface waves is confirmed by the spectral analysis of a typical raw shot gather displayed in Fig. 4. In the near-offset range, the spectrum is dominated by surface waves with a peak frequency of ~ 30 Hz (Fig. 4b), whereas the region of the shot gather containing possible reflections is dominated by a peak frequency of ~ 60 Hz (Fig. 4c).

On the basis of information presented in Figs. 3 and 4 and a careful study of all 859 raw and semi-processed shot gathers, we conclude that events R1–R3 are likely to be reflections; R1 and R2 are observed on data recorded across the landfill, whereas R3 is observed on data acquired over natural ground. All three events can be followed over a large number of sequentially recorded shot gathers and have move-outs that differ markedly from the source-generated noise (Fig. 3). Their nonhyperbolic shapes or limited extents on many shot gathers can be explained by the presence of substantial lateral velocity heterogeneity.

## 5. Seismic reflection data processing

Our seismic data have been processed under the assumption that events R1–R3 represent the earliest

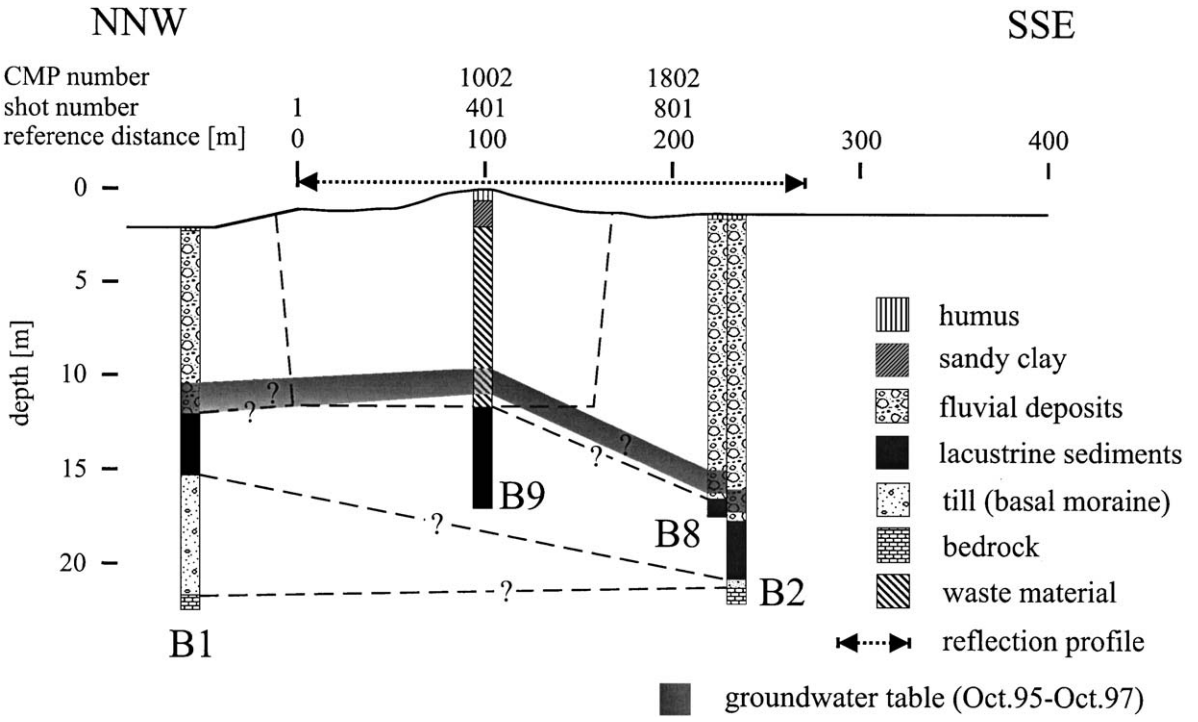


Fig. 2. Interpreted cross-section of landfill and adjacent natural ground based on information from boreholes B1, B2, B8 and B9 (Fig. 1; Kissling, 1998). Approximately 11 m of waste material in borehole B9 is covered by ~ 2 m of humus and sandy clay. Natural ground in boreholes B1, B2 and B8 comprises 0.2–0.3 m of humus underlain at progressively deeper levels by 10–16 m of fluvial deposits, 3–5 m of lacustrine sediments and 0.5–6.0 m of till. Bedrock is at ~ 20-m depth. Extent of seismic reflection profile is delineated by dotted line. Cross-section is vertically exaggerated by a factor of 10.

recorded reflections. The relatively conventional pre-stack processing included:

1. trace editing;
2. elevation static corrections and amplitude scaling using a 30-ms AGC;
3. gentle F–K filter to suppress the surface waves;
4. spectral balancing (30–45 to 250–400 Hz);
5. common midpoint (CMP) sorting (e.g. Fig. 5);
6. application of strong top-mute functions marked by dashed lines in Fig. 5;
7. velocity analysis by simply fitting hyperbolae to the R events;
8. application of normal move-out (NMO) corrections.

Refraction and residual static corrections were not applied because they did not result in improvements to the stacked section. Furthermore, the generally low quality of the CMP gathers and final stack, together with the lack of uniformly reliable velocity information (see descriptions of the tomographically derived velocity models), precluded the successful application of migrations routines.

A selection of eight CMP gathers that result from processing steps 1–6 is displayed in Fig. 5. Their locations along the length of the profile are shown in Fig. 6. CMPs 488, 510, 529, 569, 636 and 672 were chosen from shot gathers containing events R1 and R2 (Fig. 5a–f); CMP 1108 contains no notable reflected energy (Fig. 5g), and CMP 1875 was selected from shot gathers containing event R3 (Fig. 5h). Event R1 has a clearly hyperbolic shape (Fig. 5a–d). It is notable that it extends over an offset range of ~ 40 m in Fig. 5c. Its apex is ~ 8 m from the zero offset position, indicating a dipping reflector and/or significant lateral velocity variations in the shallow subsurface. By comparison, events R2 and R3 are clearly defined on less than 50% of the traces in any CMP gather (Fig. 5e, f and h). Even

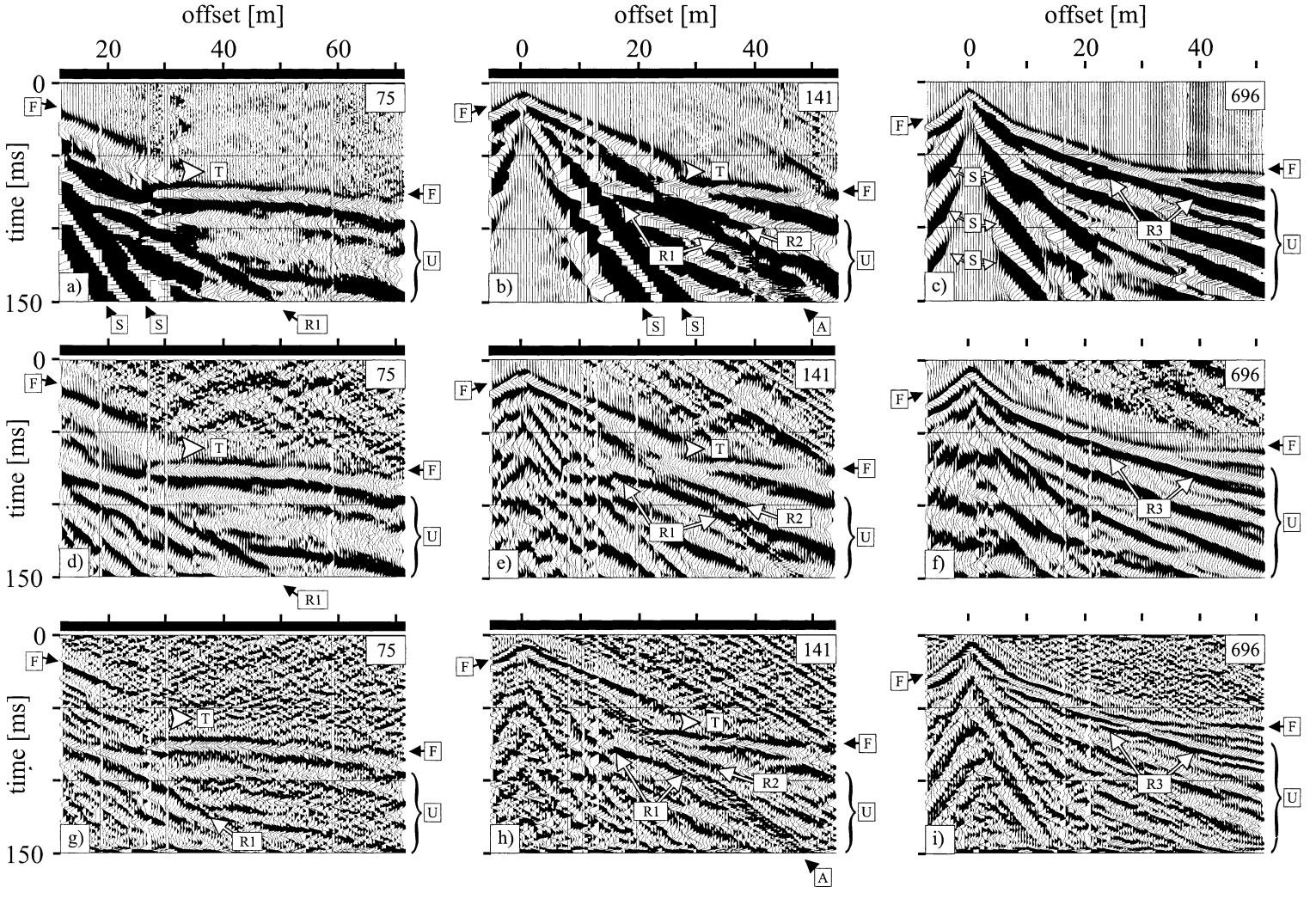


Fig. 3. (a–c) Typical trace-equalised raw shot gathers 75 and 141 recorded over the landfill and shot gather 696 recorded over natural ground. Every second trace of 240-channel shot gathers 75 and 141, and every trace of 120-channel shot gather 696 has been plotted. Gain and plot parameters chosen to emphasise variable quality of first breaks. Position of landfill is marked by black bar at top of shot gathers. (d–f) As for (a–c), after application of 30 ms AGC and gentle F–K filter. (g–i) As for (a–c), after application of 30 ms AGC and spectral whitening (30–45 to 250–400 Hz). A, airwave; F, first breaks; R1–R3, possible reflections; S, surface waves (ground roll); T, traveltime offset; U, guided waves.

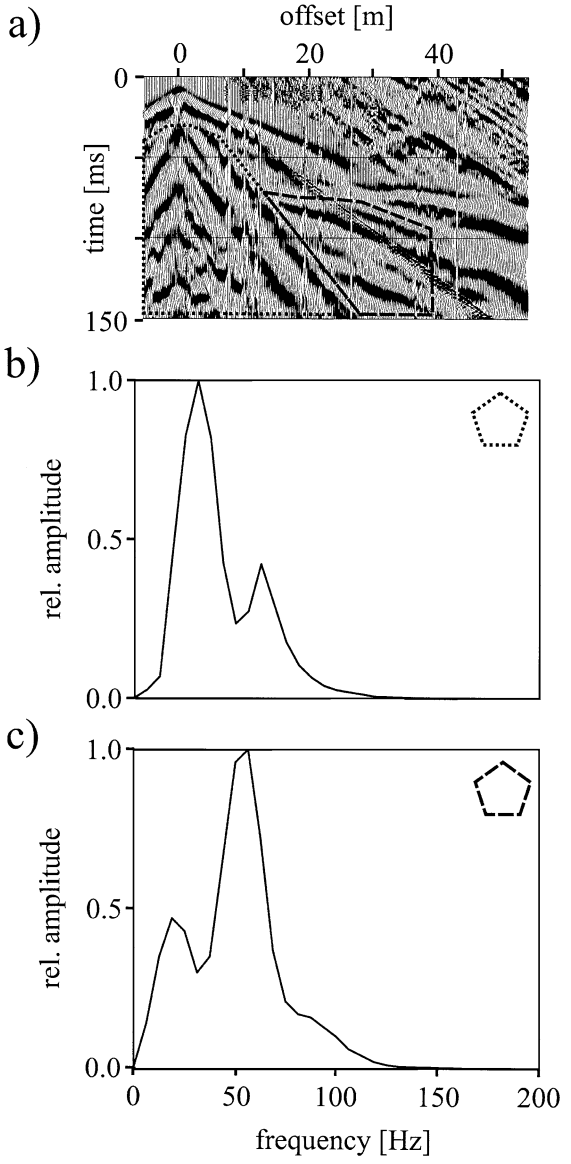


Fig. 4. Spectral analysis of typical shot gather 141 (Fig. 3b). (a) Raw shot gather. Analysed area outlined by dotted line is dominated by surface waves. That delineated by dashed line contains possible reflections. (b) Spectrum of region dominated by surface waves showing peak at ~ 30 Hz. (c) Spectrum of region containing possible reflections and multiples showing peak at ~ 60 Hz.

so, the NMO velocities and zero-offset traveltimes obtained by fitting hyperbolae to events R1–R3 are shown in the upper right corners of the CMPs in Fig. 5. Because of the limited offset ranges over which the events can be identified, these velocity estimates are poorly constrained.

Stacking of the CMP-sorted data followed by bandpass filtering (30–45 to 100–150 Hz) results in the section displayed in Fig. 6. Event R1 extends from distance ~ 20 to ~ 50 m, R2 from ~ 50 to ~ 105 m and R3 from ~ 160 to ~ 240 m at the end of the line. Since other coherent features on this section could not be confidently identified on the raw and processed prestack data, we are reluctant to interpret them as true reflections.

To interpret the seismic reflection section, it was necessary to correlate events R1–R3 with the depths to boundaries identified in boreholes B2, B8 and B9. Conversion of the R1–R3 traveltimes (as shown in Fig. 6) to depths required reliable velocities. Unfortunately, analyses of the reflections in the prestack data did not provide sufficiently consistent velocity estimates to perform the time-to-depth conversions. For example, when reflection traveltimes were converted to depths using the poorly constrained NMO velocities, inconsistent correlations between reflections and subsurface boundaries resulted. At this stage of our analysis, we concluded that independent estimates of subsurface velocities were required. We anticipated that straightforward tomographic inversions of first-arrival times would provide the necessary information.

## 6. Picking, inverting and ray tracing

### 6.1. Picking first-breaks

An automatic first-break picker (ProMAX, 1997) was used to determine initial estimates of first-arrival times. Low signal-to-noise ratios required these estimates to be adjusted manually for nearly all far-offset (>20 m) traces recorded over the landfill (Fig. 3a–b). Reliable first-arrival times with an average error varying from less than $\pm 0.5$ ms in the near-offset range to $\pm 1.0$ ms in the far-offset range were obtained for ~ 183,000 traces.

### 6.2. Tomographic inversion (refracted arrivals)

To determine subsurface velocities from first-arrival times, we use a tomographic algorithm that employs a fast finite-difference eikonal solver for calculating

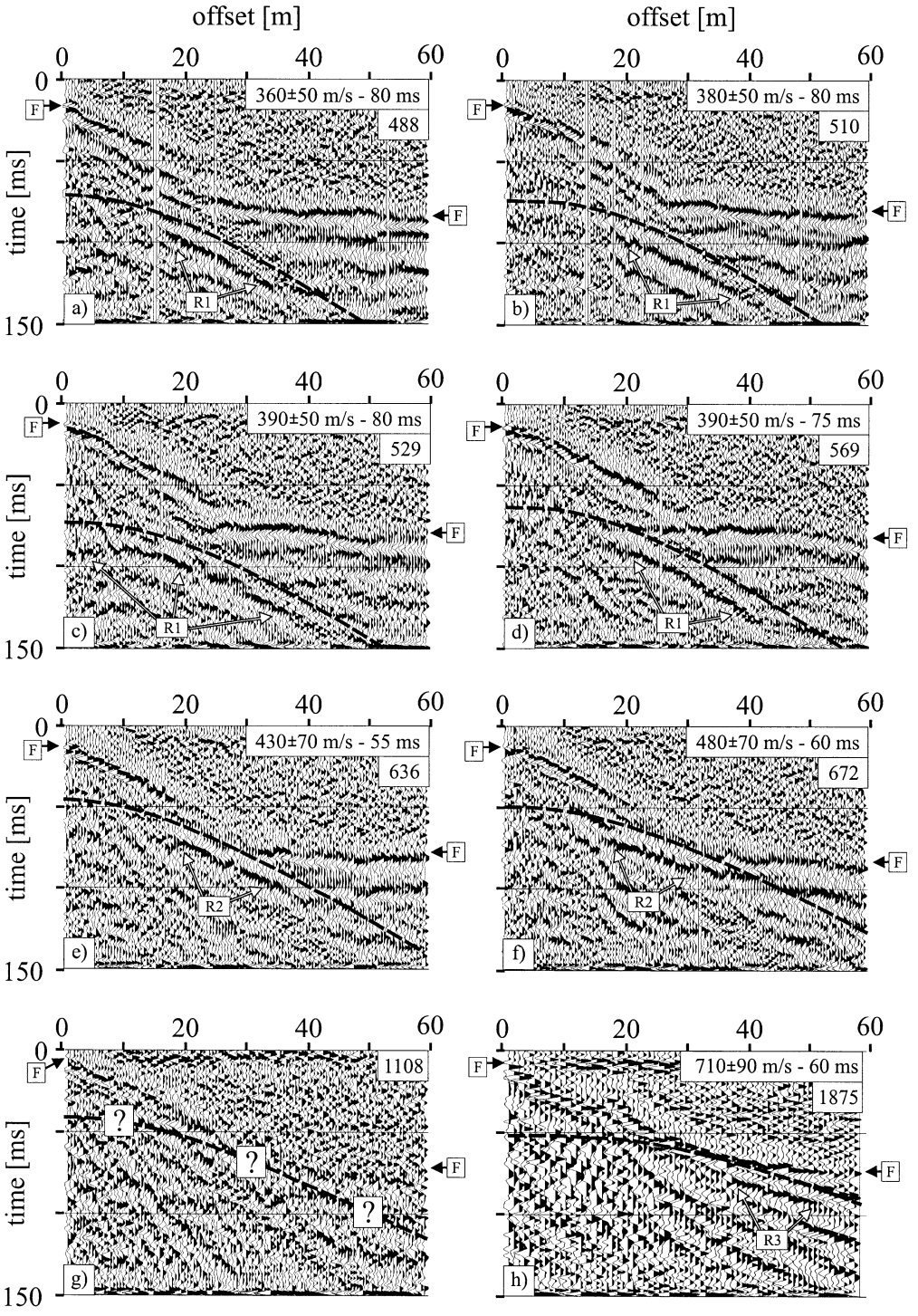
offset [m]
0
20
40
60
time [ms]
150
360±50 m/s - 80 ms
488
380±50 m/s - 80 ms
510
390±50 m/s - 80 ms
529
390±50 m/s - 75 ms
569
430±70 m/s - 55 ms
636
480±70 m/s - 60 ms
672
1108
710±90 m/s - 60 ms
1875
F
R1
R2
R3
?
a)
b)
c)
d)
e)
f)
g)
h)

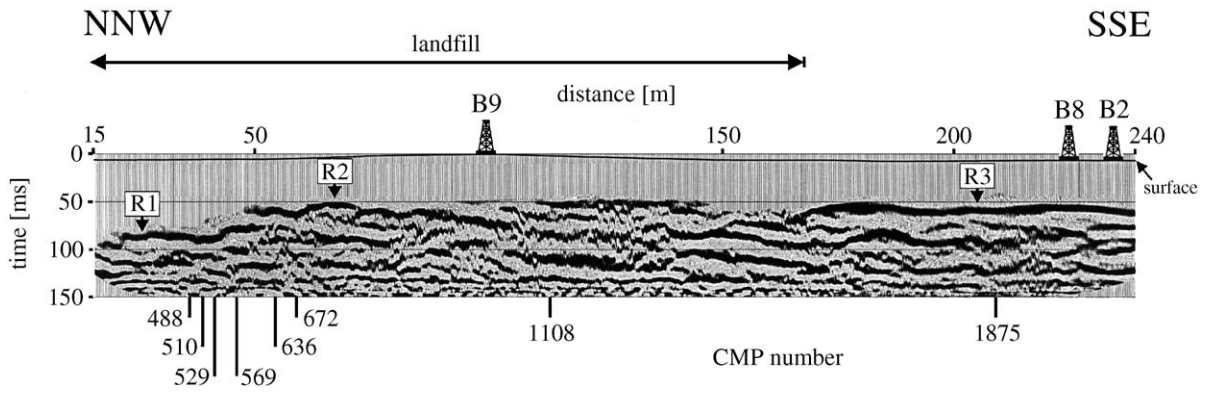


Fig. 6. Stacked section. Processing included elevation static corrections, AGC (30 ms window), F–K filter, spectral whitening (30–45 to 250–400 Hz), top-mute, NMO corrections, CMP sorting, stacking and bandpass filter (30–45 to 100–150 Hz). Positions of CMP gathers displayed in Fig. 5 are marked at bottom of section. R1–R3, possible reflections. Datum is defined by highest point of survey area (431.1 m at borehole B9). Maximum elevation change is 1.5 m.

traveltimes and raypaths in 2-D heterogeneous media and an LSQR inversion scheme (Paige and Saunders, 1982; Schneider et al., 1992; Lanz et al., 1998). Data sets that require tomographic inversion invariably include an underdetermined component, such that not all model parameters can be unambiguously constrained. Underdetermined problems can be forced to be formally unique by supplying appropriate regularization constraints. Here, we apply the smoothing constraints of Constable et al. (1987) to ensure model simplicity and the damping constraints of Marquardt (1970) to moderate deviations during each iteration. To start the inversion process, an initial input model is needed (e.g. a homogeneous medium or a model defined by a velocity at the surface and a vertical gradient, etc.).

A model consisting of $270 \times 35$ grid points for the forward calculation of traveltimes and $540 \times 70$ grid points for the inversion process requires a memory allocation of $\sim 13$ Mb and a calculation time per iteration of approximately 10 h on a SUN Server Enterprise-450 (300 MHz processor). Because of strong nonlinearities, numerous iterations may be required to achieve convergence. For example, our preferred Model 3 required 23 iterations or $\sim 230$ h (9.6 days) of computation. In its current form, the tomographic scheme only inverts the times of direct and refracted arrivals.

### 6.3. Ray tracing refracted and reflected arrivals

Tomographic inversions are only as good as the data on which they are based. It is well known that areally extensive low-velocity layers and thin high-velocity layers may not be represented by first-arrivals. To determine information on such features requires the analysis of amplitudes and/or the interpretation of secondary arrivals, including vertical-incident and wide-angle reflections. For the joint analysis of first and secondary arrivals, we employ a ray-tracing program that was originally designed for interpreting 2-D crustal refraction/wide-angle reflection data (Zelt and Smith, 1992). Rays are traced through velocity models in a shooting or search mode using zero-order asymptotic ray theory. A damped least-squares technique may be used to solve the inverse problem. Positions of nodes specifying each layer can be completely general, provided the layer boundaries cross the entire model without intersecting another layer.

Fig. 5. Typical CMP gathers with elevation static corrections, AGC (30 ms window), gentle shot-domain F–K filter and spectral whitening (30–45 to 250–400 Hz) applied. Locations of CMPs shown in Fig. 6. (a–g) CMPs 488, 510, 529, 569, 636, 672 and 1108 were recorded within landfill boundaries. (h) CMP 1875 was recorded outside. Fitting of hyperbolae to R events yielded NMO velocities and zero-offset times shown in upper right corner of gathers. The same hyperbolae, but time-shifted by $-10$ ms, defined top-mute functions (shown by dashed lines) that eliminated most direct-, refracted- and guided-wave energy. F, first breaks; R1–R3, possible reflections. No reflections identified on CMP gather 1108.

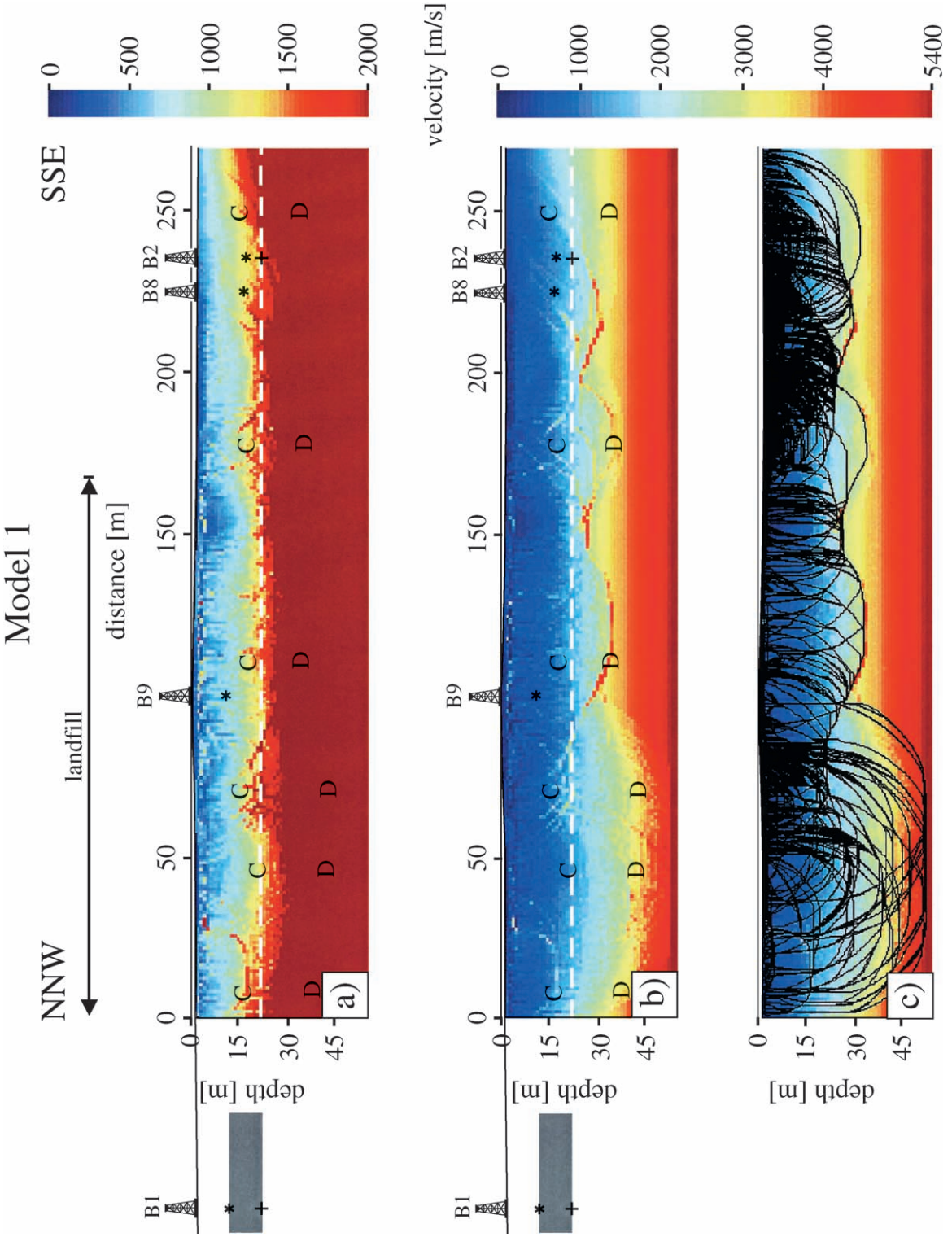
Model 1
NNW
SSE
landfill
distance [m]
velocity [m/s]
depth [m]
B1
B9
B8
B2
a)
b)
c)
C
D

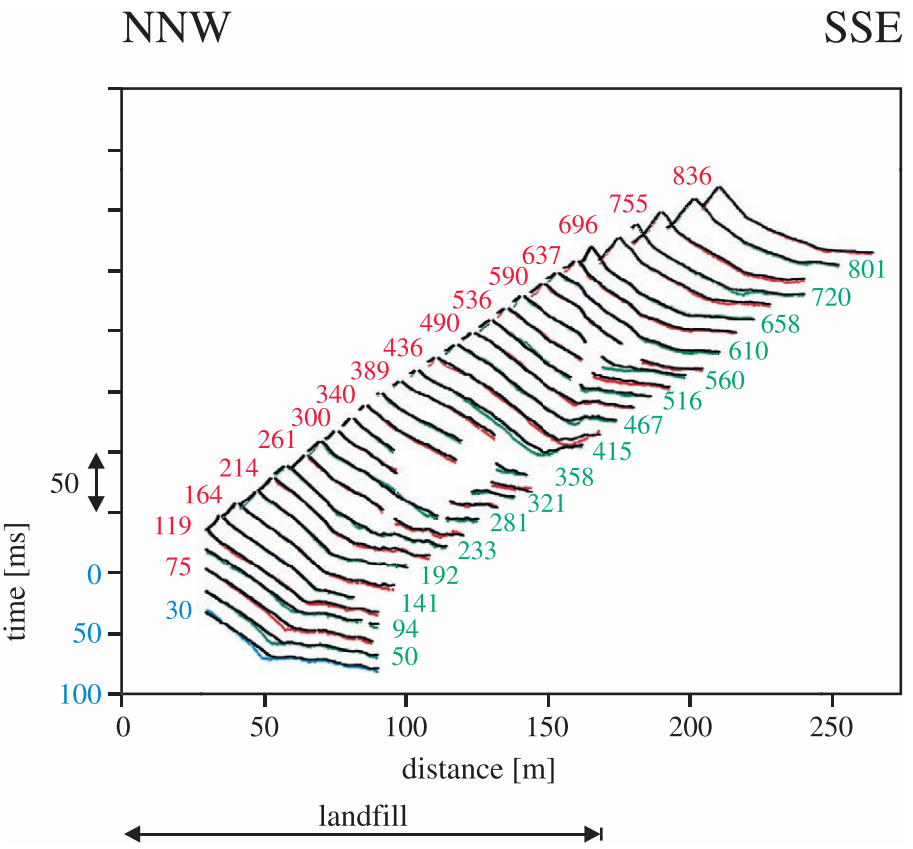


Fig. 8. For selected shot and receiver spreads distributed along entire profile (Figs. 1 and 2), traveltimes calculated for Model 1 (black lines) are compared to recorded traveltimes (blue, green and red lines). Except for spread 30 (blue), all traveltime curves are shifted 10 ms with respect to preceding one for display purposes.

For a large number of nodes, ray tracing takes a few seconds, whereas inversion may require several minutes on a SUN Server Enterprise-450 (300 MHz processor).

## 7. Gradient input model

### *7.1. Tomographic inversion results*

A simple 1-D model with a velocity of 400 m/s at the surface and a gradient of 100 m/s/m was used as input for the first suite of tomographic inversions. To obtain a meaningful result within a reasonable running time, the grid size was set to $1 \times 1$ m for the forward calculations of traveltimes and $0.5 \times 0.5$ m for the inversions. A series of tests was conducted to determine optimum values for smoothing and damping. Only a small amount of regularization was required to obtain a stable solution for the gradient input model. Inversion was constrained 97.9% by the data, 0.1% by smoothing and 2% by damping.

The resultant Model 1 and associated raypaths after twelve iterations are displayed in Fig. 7. The close

Fig. 7. Model 1 based on results of tomographically inverting all first-arrival times using a simple gradient model as input. (a) Colour scale ranges from 0 to 2000 m/s to emphasise velocities in upper part of model. (b) Colour scale ranges from 0 to 5400 m/s to emphasise velocities in lower part of model. (c) As for (b), with corresponding ray paths. Cs and Ds identify relatively abrupt velocity increases to >1700 and >3200 m/s, respectively. Stars and crosses indicate, respectively, depths to lacustrine sediments and bedrock measured in boreholes. White dashed line connects bedrock intersected in boreholes B1 and B2.

correspondence between calculated and picked first-arrival times along the length of the profile is demonstrated in Fig. 8; the RMS deviation between calculated and all observed first-arrival times is only 1.6 ms. In the upper ~ 15 m of the model, velocities are uniformly low, mostly ranging from ~ 400 to ~ 1100 m/s (Fig. 7a). Velocities increase abruptly to ≥ 1700 m/s across interface C at 15–22 m depth. They increase to >3200 m/s across the broad undulating zone D at 25–40 m depth (Fig. 7b).

### 7.2. Contradictions between Model 1 and other data

Unfortunately, critical features of Model 1 are incompatible with information provided by the four geological logs (Fig. 2), three-dimensional georadar data recorded at the same site (De Iaco et al., 2000) and the seismic reflection section (Fig. 6). Although interface C is nearly coincident with the upper surface of lacustrine sediments intersected in boreholes B2 and B8 and mapped by the georadar data, it is ~ 8 m deeper than the same surface observed in borehole B9 (Fig. 7). Moreover, there is little or no evidence in Model 1 for the anticipated velocity change at the landfill's southern margin, and the 2000 m/s velocity near the base of borehole B2 is far too low for the limestone bedrock there. Without constraints provided by the boreholes, the broad undulating zone D might have been erroneously interpreted as the bedrock boundary.

Predicted vertical-incident traveltimes to interface C are inconsistent with the seismic reflection section along >60% of its length. Vertical-incident traveltimes of reflections originating from interface C nearly match those of reflection R3 over the southeastern third of the section (Fig. 9a), but there seems to be little or no correlation between interface C and reflections R1 and R2. Further evidence that Model 1 is unreliable is provided by the unrealistic image displayed in the time-to-depth converted seismic reflection section of Fig. 9b; after time-to-depth conversion based on Model 1 velocities, relatively simple structures become exceedingly complex with numerous unexplained undulations.

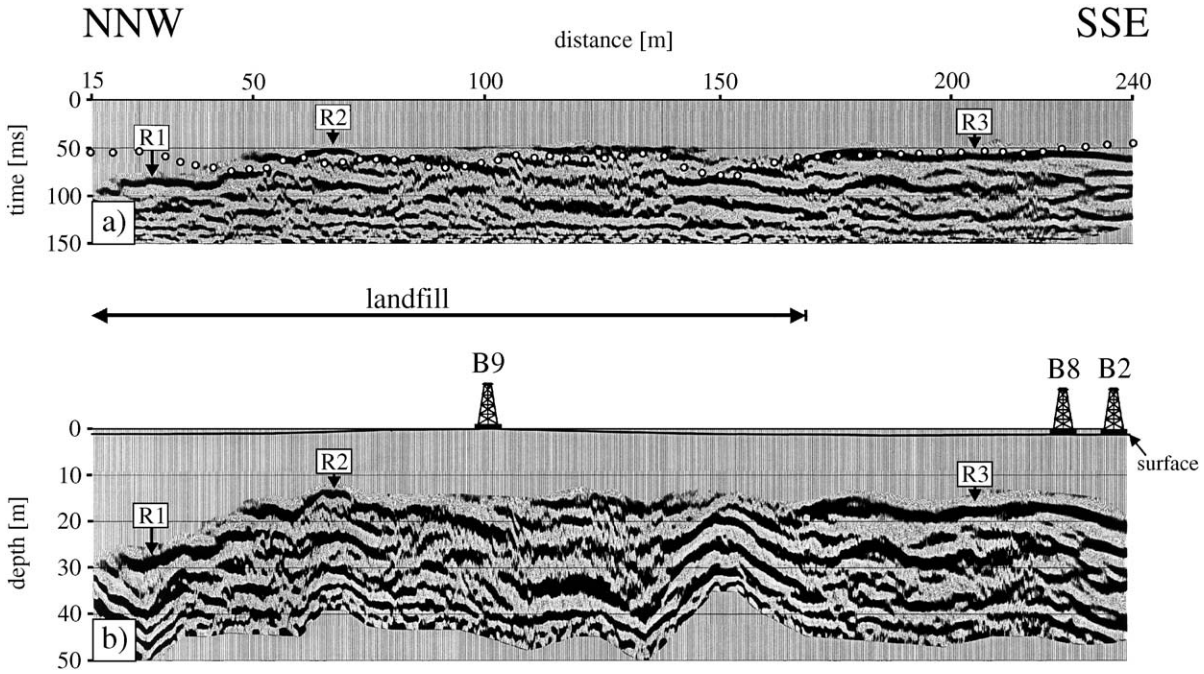


Fig. 9. (a) Two-way traveltimes to interface C of Model 1 (dots) superimposed on stacked section of Fig. 6. (b) Time-to-depth converted seismic section using average velocities obtained from Model 1. Note unrealistic pull-ups of structures (e.g. centred at lateral positions ~ 70 and ~ 150 m) due to strong lateral velocity variations of Model 1.

## 8. Trial-and-error Model 2

### *8.1. Ray trace modelling refracted and reflected arrivals*

In a first attempt to overcome the flaws of Model 1, we employed the inversion routine of Zelt and Smith's (1992) ray-tracing program to search for a model that explained the traveltimes of all first arrivals and all reflections. It was a disappointment to discover that the otherwise robust inversion procedure failed to converge satisfactorily, probably because of difficulties in defining model parameters that account for the extreme variability of traveltimes.

Using the same program, we then forward-modelled simultaneously the traveltimes of first-arrivals and reflections recorded on a small number of shot gathers (i.e. 75, 119, 141 and 696). Critical boundaries in the initial and final models were constrained to match approximately the depths to interfaces intersected in the boreholes (Fig. 2). The painstaking forward-modelling exercise resulted in velocity model 2 (not shown here) with a laterally extensive ~ 2.0-m thick surface layer of humus and sandy clay characterised by moderately low velocities (350–950 m/s) overlying the landfill with variable but generally low velocities (150–570 m/s) in the north and the fluvial deposits with moderately low velocities (350–740 m/s) in the south. In model 2, the lacustrine sedimentary unit and till were represented by intermediate velocities (2800–4100 m/s) and the bedrock had relatively high velocities (5200–5400 m/s). Since only a small fraction of the first arrivals were included in the modelling, the first arrival times observed on the majority of shot gathers were only poorly predicted by model 2.

## 9. Refined Model 3

### *9.1. Tomographic inversion results*

To reduce the misfit between synthetic and observed first-arrival times, Model 2 was used as input for a second suite of tomographic inversions in which certain parts of the model were prevented from markedly changing unless there were compelling reasons to do so. Limiting the inversion process to make only minor changes during any single iteration step was achieved by employing moderately high damping constraints. Above the top of the lacustrine layer, the percentages of data, smoothing and damping constraints were set to 94.9%, 0.1% and 5%, respectively, whereas those at and below this interface were set to 79.9%, 0.1% and 20%. With these regularization parameters, changes in layer thickness and velocity were forced to occur mostly within the heterogeneous waste and fluvial deposits. Because rays travelling through these near-surface low-velocity layers were almost vertical, the thicknesses and velocities within these layers were interdependent, such that traveltimes could be matched by maintaining the thicknesses and simply adjusting the velocities. As a result of this procedure, depths to the lacustrine sediments in the vicinity of the boreholes remained near to their input values.

Model 3, which was obtained after 23 iterations, is the result of the second suite of tomographic inversions (Fig. 10). Except for some minor artefacts at a distance of ~ 120 m, it explains the observed first-arrival times almost as well as Model 1 does (compare Fig. 11 with Fig. 8). The RMS deviation between calculated (based on Model 3) and observed first-arrival times is only 2.1 ms.

All of the expected structural features are contained in Model 3. Overlying the landfill is a thin surficial layer of humus and sandy clay with velocities of 400–1000 m/s. Throughout the landfill itself, velocities are mostly lower than those above, with values varying between 200 m/s and 600 m/s. The southern boundary of the landfill is now distinguished by fairly abrupt increases in velocity from ~ 350 to ~ 600 m/s.

Across undisturbed natural ground, the thin low-velocity humus layer is underlain by fluvial deposits with velocities that increase southwards from ~ 600 to 900 m/s at the end of the line. Although velocities and depths to the lacustrine sediments and bedrock changed somewhat relative to the Model 2 input values, the correct depths in the vicinity of the boreholes have been preserved. The model predicts a minor southward thickening of the fluvial deposits and a corresponding minor southward thinning of the lacustrine sediments and basal till layer, but the upper surface of the bedrock (interface D″ in Fig. 10) appears to be nearly horizontal. Velocities of the lacustrine sediments and basal till layer vary between

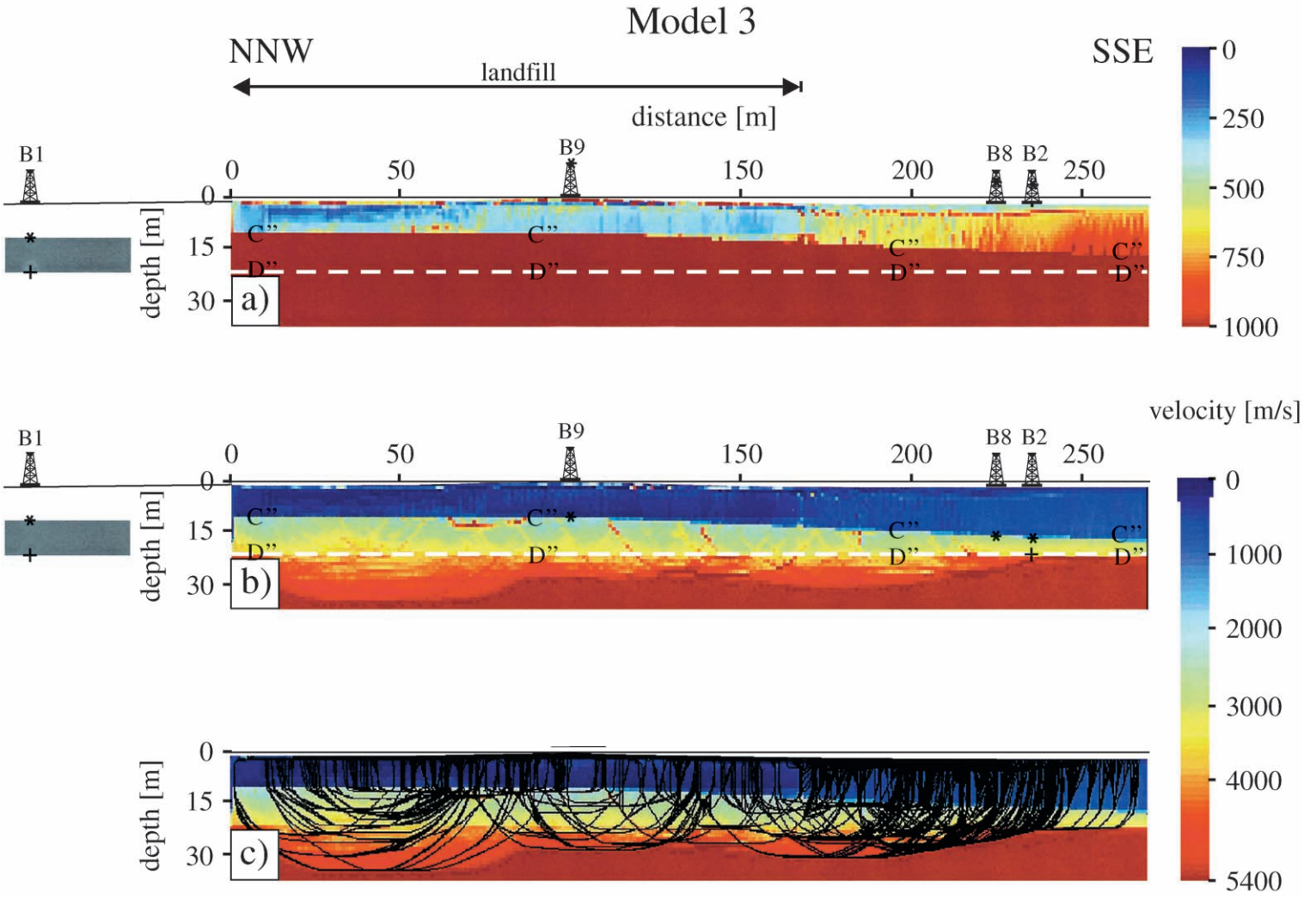


Fig. 10. Final Model 3 based on results of tomographically inverting all first-arrival times using Model 2 as input (see text). (a) Colour scale ranges from 0 to 1000 m/s to emphasise velocity variations in upper part of model. (b) Colour scale ranges from 0 to 5400 m/s to emphasise velocity variations in lower part of model. (c) As for (b), with corresponding ray paths. During inversion, depths to top of lacustrine sediments (C″) and top of bedrock (D″) were constrained to vary less than other parts of input model. Stars and crosses indicate, respectively, depths to lacustrine sediments and bedrock measured in boreholes. White dashed line connects bedrock intersected in boreholes B1 and B2.

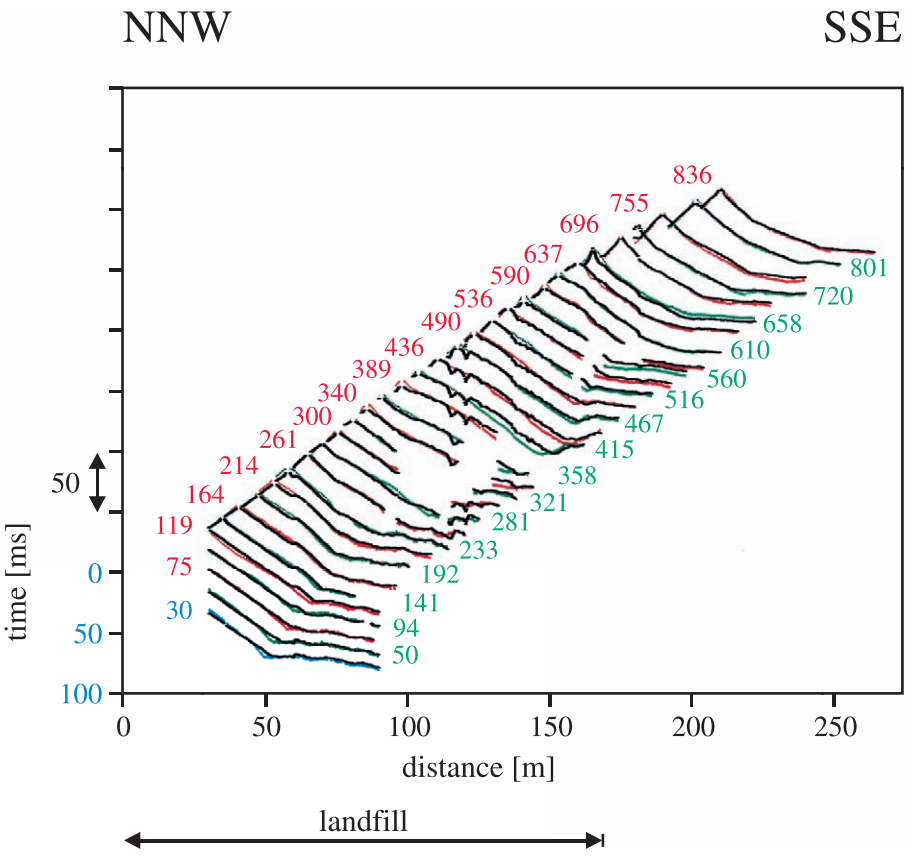


Fig. 11. As for Fig. 8, except for final Model 3.

2000 and 3800 m/s. Bedrock velocities vary both laterally and vertically within the range 4000–5400 m/s, values that are consistent with the presence of Lower Freshwater Molasse siltstone and the Upper Jurassic limestone (Knödel et al., 1997).

### 9.2. Combining the results of the reflection and refraction analyses

Zero-offset traveltimes of waves reflected at interface C″, the top of the lacustrine sediments, are superimposed on the stacked time section in Fig. 12a, and the associated time-to-depth converted section using Model 3 velocities is presented in Fig. 12b. On the basis of Fig. 12a, it appears that R1 and R3 and a portion of R2 are reflections from the top of the lacustrine sediments. In the region where reflections R1 and R2 overlap, interface C″ seems to correspond to reflection R1. Although there is little doubt that reflections R1 and R2 do indeed overlap in our data (e.g. see shot gather in Fig. 3e and h), it is possible that reflection R1 originates from the upper surface of lacustrine sediments directly beneath the profile, whereas a portion of reflection R2 originates from the same undulating boundary, but from out-of the plane, or vice versa.

Unlike Fig. 9b, reflections in the depth section of Fig. 12b are relatively simple, comparable in form to the time section. Except for the distance ranges 55–72 and 120–160 m, the upper surface of lacustrine sediments seems to have been imaged by distinct reflections. Since this surface also corresponds to the base of the former gravel deposit in the region of the landfill, we conclude that the combined seismic reflection–refraction analysis has allowed the (maximum) thickness of waste material to be determined over the northern two-thirds of the landfill. It is noteworthy

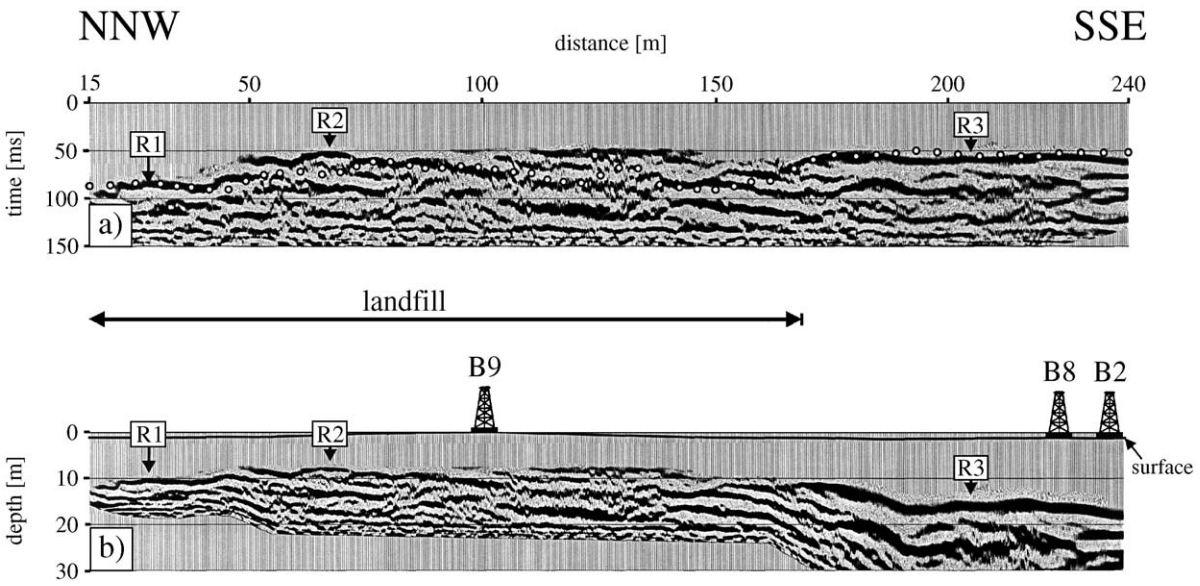


Fig. 12. As for Fig. 9, except for Model 3. Pull-ups of structures between 15 and 170 m is due to low-velocity waste material. Note smooth variations of depths to reflectors in (b) relative to those in Fig. 9b.

that the high velocities ( ~ 3800 m/s) at the base of the combined lacustrine sediments–basal till layer approach those ( ~ 4000 m/s) at the top of the underlying basement rocks, perhaps explaining the weakness or absence of a reflection from their mutual interface.

## 10. Conclusions

The principal objectives of our seismic investigation were to delineate the base of the disused Härkingen landfill and to map the geometries of the host sediments (Figs. 1 and 2). To achieve these goals, a shallow seismic reflection data set with high fold ($\geq$120 in central regions of the profile) and high resolution (0.125-m CMP spacing) was recorded across the landfill and adjacent natural ground. Reflections with characteristic hyperbolic shapes were observed on only a limited number of the acquired raw shot gathers, primarily due to the overwhelming effects of source-generated noise (i.e. direct, refracted, guided and surface waves) and the extreme lateral velocity heterogeneity of the buried waste. After F–K filtering and spectrally balancing the data, a visual examination of all 859 processed shot gathers revealed three events R1–R3 that had moveouts substantially different from those of the source-generated noise. They were observed on large numbers of sequentially recorded shot gathers. By fitting hyperbolae to these events in the CMP domain, it was possible to determine stacking velocities and define top-mute functions that removed most of the direct-, refracted- and guided-wave energy. At this stage, we concluded that events R1–R3 were, in all likelihood, reflections. After applying a relatively conventional processing sequence, the stacked seismic reflection section of Fig. 6 was obtained.

Initial attempts to match reflections R1–R3 (Fig. 6) with geological boundaries in nearby boreholes (Fig. 2) were impeded by a lack of dependable velocity information. Converting the R1–R3 traveltimes to depths using the poorly constrained NMO velocities resulted in contradictory correlations. Major differences between NMO velocities (which should optimise the coherency of the stacked section) and formation velocities (which are required to convert traveltimes to depths) were doubtless caused by the high level of lateral heterogeneity in the region; at some locations in the final tomographic model, shallow velocities varied by a factor of three over the length of the recording spread (Fig. 10a).

To determine velocities throughout the region of interest, first-arrival times were inverted using a tomographic scheme that had been employed successfully by Lanz et al. (1998) at the Stetten landfill in northern Switzerland. Based on ~ 183,000 first-arrival times and a simple gradient input model, tomographic inversion using low levels of smoothing and damping produced Model 1 of Fig. 7. Although the RMS deviation between computed and observed first-arrival times was a mere 1.6 ms (see also Fig. 8), there were numerous inconsistencies between Model 1 and information provided by the boreholes, three-dimensional georadar data and the seismic reflection section:

1. a prominent increase in velocity (interface C) coincided approximately with the depth to lacustrine sediments in boreholes B2 and B8, but not with that in borehole B9;
2. the predicted velocity near the base of borehole B2 was too low for the limestone bedrock intersected there—the shallowest occurrence of velocities typical of basement rock was far too deep;
3. the southern landfill boundary was not represented by a velocity change;
4. there was only a poor correspondence between interface C and the vertical-incident reflections R1–R3 (Fig. 9a);
5. time-to-depth conversion of the seismic reflection section using Model 1 velocities yielded an unreasonably complex subsurface image (Fig. 9b).

Problems with Model 1 may have been the result of an inappropriate input model and/or a break-down in one of the key assumptions of standard refraction tomography: that all layers in the subsurface are adequately represented by first-arrivals. It is well known that seismic waves travelling through laterally extensive low-velocity layers or thin high-velocity layers may not be recorded as first arrivals. To address these issues, we employed a simple forward modelling scheme to derive Model 2 (not shown here), which explained the traveltimes of first arrivals and reflections R1–R3 on a selection of shot gathers and at the same was consistent with information provided by the boreholes and three-dimensional georadar data.

The final stage of our investigation involved using Model 2 as input for a new round of first-arrival traveltime inversions. To prevent the depths to the lacustrine sediments from deviating significantly from those observed in the boreholes, moderately high levels of damping were imposed at selected locations of the model. In this way, most of the critical adjustments during the inversion were made to velocities above the lacustrine sediments. The resulting Model 3 incorporated all important units observed in the boreholes at their correct depths and provided velocities in the expected ranges (Fig. 10). These included (i) a surface layer of humus and sandy clay (400–1000 m/s), (ii) a distinct low-velocity waste body (200–600 m/s), (iii) fluvial deposits (600–900 m/s), (iv) a combined lacustrine sediments–basal till layer (2000–3800 m/s) and (v) bedrock (4000–5400 m/s). First-arrival times computed for Model 3 matched the recorded times almost as well as those of Model 1 (RMS deviation of 2.1 versus 1.6 ms; also compare Fig. 11 with Fig. 8). Moreover, a comparison of vertical-incident traveltimes to boundaries in Model 3 with the seismic reflection section (Fig. 12a) demonstrated that reflections R1–R3 probably originated from the upper surface of the lacustrine sediments. Beneath the northern 60% of the seismic profile, this upper surface likely corresponded to the base of the landfill. Finally, time-to-depth conversion of the seismic reflection section using Model 3 velocities produced a plausible subsurface image (Fig. 12b).

Our study has demonstrated that neither the 2-D seismic reflection technique nor the 2-D seismic refraction technique, on their own, were capable of meeting the principal objectives at the Härkingen study site. In contrast, when results from the two methods were combined and suitable constraints from borehole and other data were incorporated, essential details concerning the landfill and host sediments were resolved. This successful outcome was the result of very considerable expenditures of effort in data acquisition, data processing and modelling. Moreover, shortcomings associated with employing 2-D seismic refraction and reflection methods for resolving problems in highly heterogeneous three-dimensional media were underscored during the course of this investigation.

## Acknowledgements

We thank Peter Jordan for proposing the Härkingen landfill as an appropriate study site, and for his

assistance in resolving numerous logistical problems. We also thank Michael Roth for numerous valuable discussions, Olivier Kissling for providing information on the geology and hydrogeology of the study site and local farmers Toni Bläsi, Roman Hauri and Markus Moll for providing access to their farmland. This project was supported by grants from ETH Zurich and the Swiss National Science Foundation.

## References

Boyce, J.I., Eyles, N., Pugin, A., 1995. Seismic reflection, borehole and outcrop geometry of Late Wisconsin tills at a proposed landfill near Toronto, Ontario. Can. J. Earth Sci. 32, 1331–1349.

Büker, F., Green, A.G., Horstmeyer, H., 1998. Shallow seismic reflection study of a glaciated valley. Geophysics 63, 1395–1407.

Cardarelli, E., Bernabini, M., 1997. Two case studies of the determination of parameters of urban waste sites. J. Appl. Geophys. 36, 167–174.

Constable, S.C., Parker, R.L., Constable, C.G., 1987. Occam's inversion: a practical algorithm for generating smooth models from electromagnetic sounding data. Geophysics 52, 289–300.

Dana, D., Zelt, C., Levander, A., 1999. High-resolution seismic survey over a near-surface contamination site. 69th Ann. Intern. Mtg. Soc. Expl. Geophys., Expanded Abstracts. Society of Exploration Geophysics, Tulsa, OK, pp. 579–581.

De Iaco, R., Green, A.G., Horstmeyer, H., 2000. An integrated geophysical study of a landfill and its host sediments. Eur. J. Environ. Eng. Geophys. 4, 223–263.

Doll, W.E., 1998. Reprocessing of shallow seismic reflection data to image faults near a hazardous waste site on the Oak Ridge Reservation, Tennessee. Symp. Applic. Geophys. Environ. Engin. Prob. (SAGEEP), Proceedings. Environmental and Engineering Geophysical Society, Denver, CO, pp. 705–714.

Doll, W.E., Miller, R.D., Xia, J., 1996. Enhancement of swept source near-surface seismic reflection data at a hazardous waste site. 66th Ann. Intern. Mtg. Soc. Expl. Geophys., Expanded Abstracts. Society of Exploration Geophysics, Tulsa, OK, pp. 877–879.

Granda, A., Cambero, J.C., 1998. The use of geophysical techniques for the detection and characterization of landfill in areas of urban development. 4th Ann. Mtg., Environ. Engin. Geophys. Soc., Europ. Sect., Proceedings. Environmental and Engineering Geophysical Society, European Section, Lausanne, Switzerland, pp. 111–114.

Kissling, O., 1998. Anwendung und Evaluation verschiedener Methoden im Rahmen der Voruntersuchung belasteter Standorte am Beispiel von zwei ehemaligen Deponien im Aaregäu, Kanton Solothurn (Application and evaluation of different methods for a preliminary investigation of two landfills in Aaregäu, Canton of Solothurn). Unpublished PhD thesis, ETH, Zurich.

Knödel, K., Krummel, H., Lange, G., 1997. Geophysik. Springer, Berlin.

Lanz, E., Maurer, H.R., Green, A.G., 1998. Refraction tomography over a buried waste disposal site. Geophysics 63, 1414–1433.

Marquardt, D.W., 1970. Generalized inverses, ridge regression, biased linear estimation, and nonlinear estimation. Technometrics 12, 591–612.

Murray, C., Keiswetter, D., Rostosky, E., 1999. Seismic refraction case studies at environmental sites. Symp. Applic. Geophys. Environ. Engin. Prob. (SAGEEP), Proceedings. Environmental and Engineering Geophysical Society, Denver, CO, pp. 235–244.

Paige, C.C., Saunders, M.A., 1982. LSQR: an algorithm for sparse linear equations and sparse least squares. ACM Trans. Math. Softw. 8, 43–71.

Pasasa, L., Wenzel, F., Zhao, P., 1998. Prestack Kirchhoff depth migration of shallow seismic data. Geophysics 63, 1241–1247.

ProMAX, 1997. A Reference Guide for the ProMAX Geophysical Processing Software (2D, 7.0). Advance Geophysical, Englewood, CO. Two volumes.

Robertsson, J.O.A., Holliger, K., Green, A.G., 1996a. Source-generated noise in shallow seismic data. Eur. J. Environ. Eng. Geophys. 1, 107–124.

Robertsson, J.O.A., Holliger, K., Green, A.G., Pugin, A., De Iaco, R., 1996b. Effects of near-surface waveguides on shallow high-resolution seismic refraction and reflection data. Geophys. Res. Lett. 23, 495–498.

Rodriguez, E.B., 1987. Application of gravity and seismic methods in hydrogeological mapping at a landfill site in Ontario. 1st National Outdoor Action Conference on Aquifer Restoration, Ground Water Monitoring and Geophysical Methods. Assoc. of Groundwater Sci. and Eng., Proceedings. National Water Well Association, Dublin, OH, pp. 487–504.

Roth, M., Holliger, K., Green, A.G., 1998. Guided waves in near-surface seismic surveys. Geophys. Res. Lett. 25, 1071–1074.

Schneider Jr., W.A., Ranzinger, K.A., Balch, A.H., Kruse, C., 1992. A dynamic programming approach to first arrival traveltime computation in media with arbitrarily distributed velocities. Geophysics 57, 39–50.

Slaine, D.D., Pehme, P.E., Hunter, J.A., Pullan, S.E., Greenhouse, J.P., 1990. Mapping overburden stratigraphy at a proposed hazardous waste facility using shallow seismic reflection methods. In: Ward, S.H. (Ed.), Geotechnical and Environmental Geophysics. Environmental and Groundwater, vol. II. Soc. Expl. Geophys. Society of Exploration Geophysics, Tulsa, OK, pp. 273–280.

Steeples, D.W., Green, A.G., McEvilly, T.V., Miller, R.D., Doll, W.E., Rector, J.W., 1997. A workshop examination of shallow seismic reflection surveying. The Leading Edge 16, 1641–1647.

Zelt, C.A., Smith, R.B., 1992. Seismic traveltime inversion for 2-D crustal velocity structure. Geophys. J. Int. 108, 16–34.